

CHANDRA AND XMM-NEWTON OBSERVATIONS OF THE VELA-LIKE PULSAR B1046-58

M. E. GONZALEZ^{1,2}, V. M. KASPI^{1,3}, M. J. PIVOVAROFF⁴, AND B. M. GAENSLER^{5,6}*Draft version December 2, 2024*

ABSTRACT

We present results from *Chandra* and *XMM-Newton* observations of the radio pulsar B1046-58. A high-resolution spatial analysis reveals an asymmetric pulsar wind nebula (PWN) $\sim 6'' \times 11''$ in size. The combined emission from the pulsar and its PWN is faint, with a best-fit power-law photon index of $\Gamma = 1.7^{+0.4}_{-0.2}$ and unabsorbed luminosity of $\sim 10^{32}$ ergs s $^{-1}$ in the 0.5–10.0 keV range (assuming a distance of 2.7 kpc). A spatially resolved imaging analysis suggests the presence of softer emission from the pulsar. No pulsations are detected from PSR B1046-58; assuming a worst-case sinusoidal pulse profile, we derive a 3σ upper limit for the pulsed fraction in the 0.5–10.0 keV range of 53%. Extended PWN emission is seen within $2''$ of the pulsar; the additional structures are highly asymmetric and extend predominantly to the south-east. We discuss the emission from the PWN as resulting from material downstream of the wind termination shock, as outflow from the pulsar or as structures confined by a high space velocity. The first two interpretations imply equipartition fields in the observed structures of $\gtrsim 40$ –100 μ G, while the latter case implies a velocity for the pulsar of $\gtrsim 190$ $n_0^{-1/2}$ km s $^{-1}$ (where n_0 is the ambient number density in units of cm $^{-3}$). No emission from an associated supernova remnant is detected.

Subject headings: pulsars: general — pulsars: individual (PSR B1046-58) — X-rays: general

1. INTRODUCTION

X-ray observations of rotation-powered pulsars represent a powerful tool for studying the energetics and emission mechanisms of these objects. A large fraction of the available rotational energy is thought to be carried away in a relativistic wind of particles. When this wind is confined by the surrounding medium it decelerates and a synchrotron nebula forms, called a pulsar wind nebula (PWN). The overall PWN characteristics provide insights into the content and energy spectrum of the pulsar wind, the large-scale magnetic fields, and the surrounding medium. The small-scale structures of the nebula provide details of the acceleration sites, instabilities in the magnetic field, and the interaction between the wind and its surroundings. In young, energetic pulsars, non-thermal emission from particles accelerated in the magnetosphere and thermal emission from the surface of the star are also expected to be present.

The radio pulsar (PSR) B1046-58 was discovered during a Parkes survey of the Galactic plane (Johnston et al. 1992). It has a period of $P = 124$ ms and period derivative $\dot{P} = 9.6 \times 10^{-14}$ s s $^{-1}$. These values imply a characteristic age of $\tau_c = P/2\dot{P} = 20.4$ kyr, spin-down luminosity of $\dot{E} = 4\pi^2 I P / \dot{P}^3 = 2.0 \times 10^{36}$ ergs s $^{-1}$ (with a moment of inertia of the neutron star $I \equiv 10^{45}$ g cm $^{-2}$) and surface dipole magnetic field strength of $B = 3.2 \times 10^{19} \sqrt{P\dot{P}}$ G = 3.5×10^{12} G. These properties are similar to those of other young neutron stars typified by

the Vela pulsar. The dispersion measure of 129 pc cm $^{-3}$ towards the pulsar implies a distance of 2.7 kpc (Cordes & Lazio 2002).

Deep radio observations did not detect extended emission associated with PSR B1046-58 (Stappers et al. 1999). X-ray observations with *ASCA* and *ROSAT* detected emission near the pulsar and suggested the presence of large-scale structures surrounded by faint emission (Pivovaroff et al. 2000a). However, the poor angular resolution of these observations prevented conclusive interpretation of the data. PSR B1046-58 is also one of a few pulsars with a possible EGRET γ -ray counterpart. The EGRET source 2EG J1049-5827 is coincident with the radio coordinates of PSR B1046-58 and likely γ -ray pulsations at the radio period have been found (Kaspi et al. 2000).

Here we report on observations of PSR B1046-58 carried out with the *Chandra* and *XMM-Newton* satellites. Our study reveals a faint, arcsecond-scale PWN surrounding the pulsar. A detailed imaging and spectral analysis of the system suggests the presence of soft emission from the pulsar. We also examine the characteristics of the nebula in light of current models for the production of PWNe.

2. OBSERVATION AND DATA ANALYSIS

PSR B1046-58 was observed with *XMM-Newton* on 2002 August 10. The European Photon Imaging Camera (EPIC) MOS and PN instruments (Turner et al. 2001; Strüder et al. 2001) were operated in full- and small-frame modes, respectively. These settings provide a temporal resolution of 2.6 s for EPIC-MOS and 6 ms for EPIC-PN. The medium filters were used for MOS, the thin filter for PN. The CCD data were reduced with the *XMM-Newton* Science Analysis System (SAS v6.2.0). The standard screening criteria results in an exposure time for the MOS cameras of 20 ks. For the PN camera, only $\sim 70\%$ of the exposure time was used in the small-

¹ Department of Physics, Rutherford Physics Building, McGill University, 3600 University Street, Montreal, QC H3A 2T8, Canada.

² gonzalez@physics.mcgill.ca; NSERC PGS B.

³ Canada Research Chair, Steacie Fellow.

⁴ Lawrence Livermore National Laboratory, Livermore CA 94550

⁵ Harvard-Smithsonian Center for Astrophysics, 60 Garden Street, Cambridge, MA 02138

⁶ Alfred P. Sloan Fellow.

window mode ($4'$ field of view), resulting in an effective exposure time of 15 ks.

The *Chandra* observation of PSR B1046–58 was carried out on 2003 August 8–9. The aimpoint of the back-illuminated ACIS-S3 chip (Garmire et al. 2003) was positioned at the radio coordinates of the pulsar. The observation was taken in timed exposure, very faint mode, providing a temporal resolution of 3.2 s. The data were reduced using the CIAO 3.2.0 software and standard routines. The resulting effective exposure time was 36 ks.

The EPIC-PN instrument offers a higher sensitivity than ACIS-S, but its lower exposure time and reduced field of view limited its use to spectral and temporal analyses of the pulsar emission. In turn, the *Chandra* data were used to perform spectral and high-resolution imaging analyses of PSR B1046–58 and its surroundings, while the EPIC-MOS observations were mainly used as a consistency check due to their lower sensitivity and lower spatial resolution.

3. IMAGING ANALYSIS

Figure 1 shows the area surrounding the radio position of PSR B1046–58 obtained with *Chandra*. The image has been smoothed with a Gaussian with $\sigma=0''.5$. It reveals for the first time the detailed extended structures surrounding PSR B1046–58, which we designate as its pulsar wind nebula (PWN) based on its overall characteristics discussed in the next sections. The nebula is elongated and $\sim 6'' \times 11''$ in size, with its major axis oriented in a SE–NW direction. The line in Figure 1 marks the radio coordinates of the pulsar at $\alpha_{2000}=10^h48^m12\rlap{.}^s.6(4''.7)$ and $\delta_{2000}=-58^\circ32'03\rlap{.}''75(0''.02)$, 2σ errors (Stappers et al. 1999). While there is emission immediately surrounding the pulsar position (PWN “head”), there is also clumped emission to the SE (PWN “body”) and a bright clump to the NW (“north clump”).

The head region of the nebula is consistent with a point source surrounded by extended structures. Figure 2 shows the intensity profile of the observed emission along a $10'' \times 35''$ region in a SE–NW direction aligned with the implied axis of symmetry of the nebula. The shaded region represents the 2σ background level obtained from a nearby, source-free region. The dashed line represents *Chandra*’s PSF at an energy of 1.5 keV obtained using CALDBv3.0.3 and the *mkspsf* tool⁷. As the head region is also consistent with the radio coordinates of the pulsar, we consider the source embedded in the region to be the X-ray counterpart of the pulsar. Comparing the X-ray position of other sources in the field with their optical counterparts we derive an X-ray position for the pulsar of $\alpha_{2000}=10^h48^m12\rlap{.}^s.64$ and $\delta_{2000}=-58^\circ32'03\rlap{.}''6$, with an overall rms error of $0''.55$. This is coincident within 1σ of the radio position, especially in the more constraining declination direction (see Figure 1). We then define the “pulsar” emission as that arising in a circle of $1''$ in radius centered on the above X-ray coordinates.

⁷ The slight asymmetry in the PSF profile is due to the binning and extraction region used in order to match the profile settings for the pulsar. A small, intrinsic asymmetry in the PSF has been suggested and could also contribute (see http://cxc.harvard.edu/cal/docs/cal_present_status.html#psf).

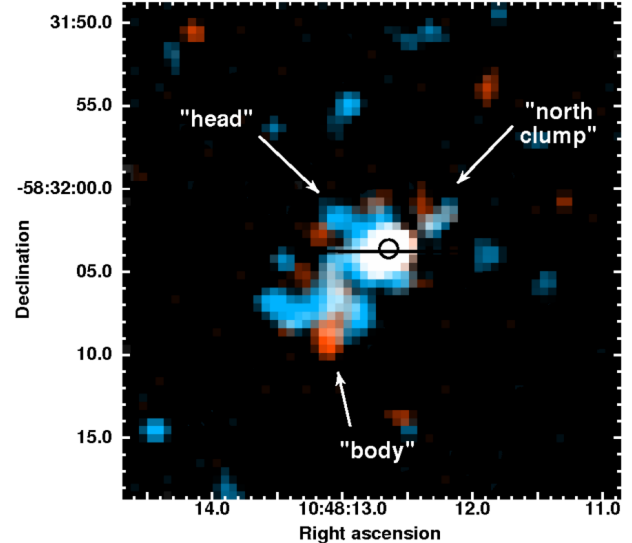


FIG. 1.— Combined *Chandra* image of PSR B1046–58 and its PWN using individual images in the 0.5–2.0 keV (red) and 2.0–10.0 keV (blue) ranges. Each image was smoothed with a Gaussian with $\sigma=0''.5$. The circle ($0''.55$ -radius) and line ($4''.7$ length) mark the X-ray and radio positions of the pulsar, respectively (see §3). The main components discussed in the text are labeled.

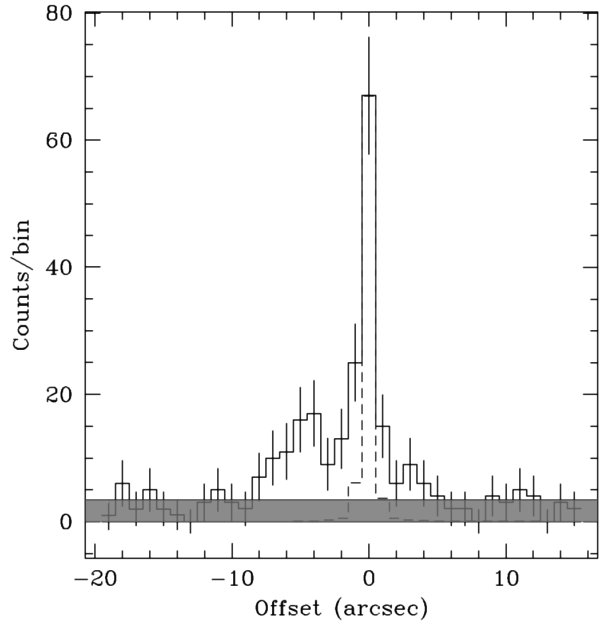


FIG. 2.— *Chandra* axial profile of PSR B1046–58 and its PWN in the 0.5–10.0 keV range in a SE–NW direction (solid line) aligned with the implied axis of symmetry (see Fig. 1). The origin represents the X-ray position of the pulsar. The extended emission at offsets of $\sim -3''$ to $-8''$ arises from the “body” of the PWN (in the SE direction) while the emission at offsets of $\sim 3''$ – $5''$ arises from the “north clump”. We also show the 2σ level of the background (shaded region) along with the PSF of the telescope at 1.5 keV (dashed line).

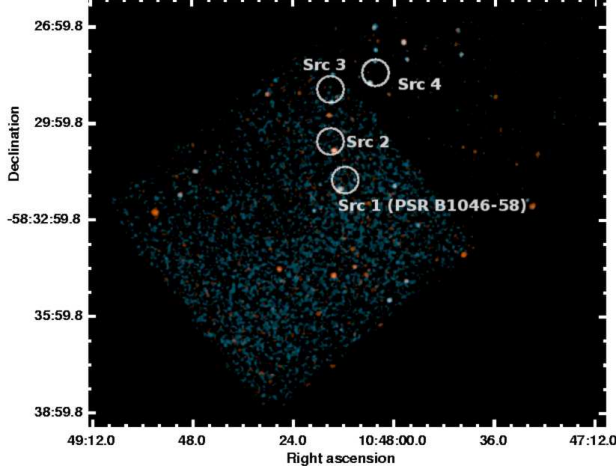


FIG. 3.— *Chandra* image of the field surrounding PSR B1046–58 obtained from the ACIS-S3 chip and part of ACIS-S2. Individual background-subtracted and exposure corrected images in the 0.5–2.0 keV (red) and 2.0–10.0 keV (blue) ranges were used. The images were smoothed with a gaussian with $\sigma=2''$. The circles mark the position of the sources detected with *ASCA* and their uncertainties (25'' radius, see Pivovaroff et al. 2000a), all of which are coincident with resolved point sources in the present observations. Similar results (although at lower angular resolution) were obtained with the *XMM–Newton* MOS instruments. No extended PWN or supernova remnant emission was detected in the data.

We also find that the extended emission from the PWN dominates at high X-ray energies. Table 1 shows the number of background-subtracted counts obtained for various parts of the system in the soft (S) and hard (H) bands, their hardness ratios ($HR = S-H / S+H$) and their total signal-to-noise ratio (S/N, e.g., Pivovaroff et al. 2000b) in the 0.5–10.0 keV range. While emission from the nebula is likely to be present within the 1'' radius used for the pulsar, we suggest that emission from the neutron star is indeed present (and may dominate) in this region. The above is supported by the fact that this region is the only one that is seen to exhibit a positive HR with high significance, suggesting a contribution of distinctly softer emission than that of the rest of the nebula.

Using *ASCA*, Pivovaroff et al. (2000a) detected four point sources within $\sim 4'$ of the radio position of the pulsar embedded in possible faint emission. The *Chandra* and *XMM–Newton* observations confirm the presence of these X-ray point sources in the field, in addition to many others resolved by *Chandra* (see Figure 3). The soft point source in *Chandra* coincident with “Src 2” from Pivovaroff et al. (2000a) has an optical counterpart in the USNO B1.0 catalog (Monet et al. 2002), while we find no counterparts for the hard sources coincident with “Src 3” and “Src 4” in present catalogues (e.g., USNO B1.0; 2MASS, Cutri et al. 2003; RASS, Voges et al. 2001). No additional extended emission was detected that can be attributed to the PWN beyond the above arc-second structures. We then conclude that the low angular resolution and broad PSF wings of the telescope significantly affected the *ASCA* observations due to the large number of point sources in the field. We also note that the *ASCA* positions appear to be systematically north of the *Chandra* coordinates, the latter being in agreement with

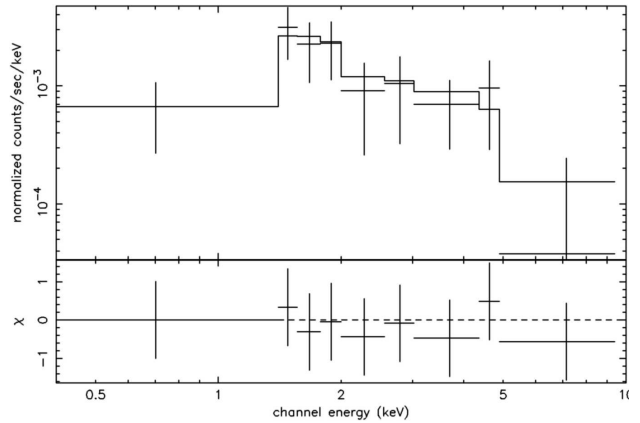


FIG. 4.— *Chandra* spectrum of the combined emission from PSR B1046–58 and its PWN. The data were binned to contain a minimum of 20 counts bin^{-1} . The solid line represents the best-fit power-law model shown in Table 2 and the lower panel shows the fit residuals.

source positions at other wavelengths.

4. SPECTRAL ANALYSIS

The data obtained from both *Chandra* and *XMM–Newton* were used to perform a spectral analysis of the emission from PSR B1046–58 and its PWN. For the *Chandra* data, an elliptical region of $12'' \times 18''$ in size was used with a surrounding annulus as background. A total of 184 ± 14 background-subtracted counts were detected in the 0.5–10.0 keV range. The *XMM–Newton* data were extracted from circular regions of 25'' radii in each detector, encompassing $\sim 77\%$ of the photons from a point source, with a nearby region used as background. The data from MOS1 and MOS2 were not included in the analysis due to the low number of counts detected in them (106 ± 17 and 47 ± 17 , respectively⁸). The PN detector collected 260 ± 47 background-subtracted counts in the same range. The extracted spectra from *Chandra*’s S3 chip and *XMM–Newton*’s PN detector were fit simultaneously in the 0.5–10.0 keV range using XSPEC (v.11.3.0) and a minimum of 20 counts per bin in each spectrum.

Thermal models for the integrated emission from the PWN and PSR B1046–58 are statistically acceptable ($\chi^2_\nu \sim 1.1$). However, they result in temperatures far too high to represent shock-heated thermal plasma ($T > 8 \times 10^7$ K, Raymond-Smith model, Raymond & Smith 1977) or emission from the surface of the neutron star ($T > 1 \times 10^7$ K, blackbody model). Instead, a non-thermal absorbed power-law model produces an equally acceptable fit (see Table 2) with a photon index of $\Gamma = 1.7^{+0.4}_{-0.2}$, similar to what is observed for other pulsars and their PWNe (e.g., Gaensler & Slane 2006). The *Chandra* spectrum with the best-fit power-law model is shown in Figure 4. The observed emission is thus consistent with having a predominantly non-thermal origin.

We then searched for differences in the spectral char-

⁸ It has been found that the MOS1 count rate can be artificially boosted by statistical fluctuations by up to $\sim 70\%$, especially for sources with < 50 true counts. See §2.1 and §4 in <http://xmm.vilspa.esa.es/docs/documents/CAL-TN-0023-2-1.ps>

acteristics of the different components of the system, as is hinted from our imaging analysis. The high spatial resolution available with *Chandra* was required in this case. The 116 ± 14 counts detected from the PWN alone were fit with a power-law model. Holding the interstellar absorption fixed to the best-fit value from Table 2, the resulting photon index was $\Gamma_{PWN} \sim 1.2$. Holding this contribution from the nebula fixed while fitting the overall spectrum, the residual (presumably pulsar-dominated) emission was well described by a power-law model with a photon index of $\Gamma \sim 2.4$. If a blackbody model is fitted to this emission the resulting temperature is $\sim 6.1 \times 10^6$ K, too high to represent purely thermal emission from the neutron star but lower than thermal fits to the overall spectrum. Although the small number of counts did not allow us to constrain the above parameters, emission from the pulsar softer than that of the nebula seems to be present.

5. TIMING ANALYSIS

The data from the *XMM-Newton* EPIC-PN camera were used to search for pulsations from PSR B1046–58. No evidence for an instrumental 1-s jump in the data was found (see, e.g., Woods et al. 2004). The dataset was converted to the solar system barycenter and a circular region of $25''$ radius centered at the above *Chandra* coordinates was used to extract the pulsar events. We also examined the dataset in different energy ranges using 0.5–10.0 keV, 0.5–2.0 keV and 2.0–10.0 keV. Radio observations of the pulsar obtained with the Parkes telescope predict a period for the middle of our observation (MJD 52496.5) of $f = 8.08512306$ Hz ($P = 123.683955$ ms).

The Z_n^2 test (Buccheri et al. 1983) was used to search for a periodic signal by folding the extracted photons over a range of 10 trial frequencies centered on the radio prediction. The number of harmonics used was varied to be $n = 1, 2, 4$, and 8. The most significant signal was found in the 0.5–2.0 keV range at $f = 8.08517(4)$ Hz (1σ error) with $Z_2^2 = 8.9$. Although this signal is consistent with the radio period of PSR B1046–58, it has a probability of chance occurrence of 6.3% for a single trial and it is not significant given the number of searches performed. Following Vaughan et al. (1994) and, e.g., Ransom et al. (2002), we can derive an upper limit on the pulsed fraction. Assuming a worse-case sinusoidal modulation, the maximum Fourier power obtained for a small range of frequencies centered on the radio prediction can be used to calculate an upper limit for the pulsed fraction at a specific level of confidence. In this way, we derive an upper limit for the pulsed fraction at the 99% confidence level of 53%, 65% and 61% in the 0.5–10 keV, 0.5–2 keV and 2.0–10.0 keV ranges, respectively.

6. DISCUSSION

6.1. PSR B1046–58

X-ray emission from young radio pulsars is expected to include contributions from any of the following processes: thermal emission from the entire surface due to initial cooling, non-thermal emission from magnetospheric processes, and possibly thermal emission from localized hot spots reheated by back-flowing magnetospheric currents (see, e.g., Kaspi et al. 2004).

The combined emission from the pulsar and its PWN is best described by a non-thermal power-law model. However, our imaging and spectral analysis suggests that an additional, soft component may be present in the pulsar’s emission. The soft emission can be well described by a steep power law with $\Gamma \sim 2.4$, although such an interpretation would contradict the generally observed trend of young pulsars having spectral indices harder than those of their PWNe (e.g., Gotthelf 2003). The additional soft emission cannot be entirely thermal, as the derived temperature is too high. It could, however, represent a combined spectrum of (hard) non-thermal plus (soft) thermal emission. The number of counts detected does not allow us to fit two-component models to this emission alone. Instead, in the case that this overall soft excess is related to thermal emission from the whole surface, we can constrain its temperature by fitting a blackbody plus power-law model and finding the maximum temperature that yields an acceptable fit to the total spectrum. We adopt hard limits for the interstellar absorption of $N_H < 2 \times 10^{22}$ cm $^{-2}$ and a blackbody radius observed at infinity of $R^\infty > 10$ km (at a distance of 2.7 kpc). The power-law index and normalization were allowed to vary freely and the maximum blackbody temperature that causes deviations from the best-fit model at the 3σ level was found. This results in a surface temperature of $T_{bb}^\infty < 1.4 \times 10^6$ K. This temperature is not constraining for cooling models of neutron stars, as the temperature in the case of minimal cooling is predicted to be $\lesssim 1.1 \times 10^6$ K for the pulsar’s characteristic age (e.g., Page et al. 2005). Similarly, if emission was present from a small polar cap on the surface with $R^\infty < 3$ km, the resulting temperature is $T_{bb}^\infty > 2.5 \times 10^6$ K. This is comparable to those seen in other pulsars (e.g., Pavlov et al. 2002) and could then explain the observed soft excess for PSR B1046–58.

6.2. The PWN

The high spatial resolution available with *Chandra* allowed us to discover the arc-second scale PWN structures surrounding the pulsar. The “head” of the nebula is coincident with the radio position of the pulsar, while diffuse emission is seen predominantly to the SE. The emission from the pulsar and PWN is very faint, with a combined unabsorbed luminosity of only $\sim 1 \times 10^{32}$ ergs s $^{-1}$ in the 0.5–10 keV range. The efficiency with which the pulsar converts its rotational kinetic energy into X-rays is then $\eta_X = L_X/\dot{E} \sim 5 \times 10^{-5}$, comparable to the values found for other Vela-like systems (e.g., Pavlov et al. 2001b; Camilo et al. 2004).

It has been recently suggested that an empirical relationship exists between the X-ray spectral power-law indices of young pulsars (Γ_{psr}) and their PWN (Γ_{pwn}) with the pulsar’s spin-down energy loss \dot{E} (Gotthelf 2003). According to this relationship, lower \dot{E} pulsars exhibit harder spectral indeces. For PSR B1046–58, the predicted values are $\Gamma_{psr} \sim 0.1$ and $\Gamma_{pwn} \sim 0.9$. The PWN emission appears to exhibit a spectrum similar to that predicted by this relationship ($\Gamma_{pwn} \sim 1.2$). However, the small number of counts and the possible detection of thermal emission limit our ability to constrain the spectral characteristics of the pulsar and its PWN. Observations of other Vela-like pulsars do not seem to support this relationship (e.g., PSR B1823–13, Gaensler et

al. 2003). However, longer observations at high angular resolution are needed to reliably test the validity of the relationship in this group of pulsars⁹.

Radio observations did not detect emission from the PWN and constraints on the radio properties depend directly on the underlying assumption for the radio efficiency ($\eta_R = L_R/\dot{E}$; Stappers et al. 1999). Detected nebulae show efficiencies in the range $\eta_R \sim 10^{-4}\text{--}10^{-3}$, while upper limits for unseen nebulae imply values of $\eta_R \lesssim 10^{-5}$ (Frail & Scharringhausen 1997; Gaensler et al. 2000). In the case of an undetected, extended radio nebula surrounding PSR B1046–58 and using a value of $\eta_R = 2 \times 10^{-4}$, the upper limit on the radio flux and required surface brightness imply a large radius of 8 pc for a circular nebula (Stappers et al. 1999). At a distance of 2.7 kpc this represents a radius of $\sim 10'$. While the X-ray size of PWNe is often found to be up to a few times smaller than the radio size due to smaller synchrotron lifetimes in the X-rays (e.g., Hester et al. 2002), we find no evidence for extended PWN structures on arcminute scales. For radio sizes $\lesssim 30''$, based on the small angular size of the X-ray nebula, the required efficiencies are very low at $\eta_R \lesssim 5 \times 10^{-7}$.

The origin of PWNe is commonly attributed to the interaction of a highly relativistic pulsar wind with its surroundings. At a radius r_s from the pulsar, representing the point of pressure balance at which the wind is confined and decelerated, we expect $P = \dot{E}/4\pi\Omega r_s^2 c$. Here, P is the surrounding pressure and $\Omega \leq 1$ is the filling factor of the wind. As the head region of the nebula is resolved as an extended structure with *Chandra*, we suggest that its outer radius can represent an upper limit on the location of the wind termination shock, while the body represents the expected emission downstream. The shock radius in this case is $r_s < 2'' = 0.026 d_{2.7}$ pc, very similar to that found for the Vela pulsar (Helfand et al. 2001) and an order of magnitude smaller than those of much more energetic pulsars such as the Crab and PSR B1509–58 (e.g., Weisskopf et al. 2000; Gaensler et al. 2002). The required pressure in this case is $P \gtrsim 8.2 \times 10^{-10} d_{2.7}^{-2}$ ergs cm^{-3} ($d_{2.7}$ is the distance to the pulsar in units of 2.7 kpc). In the region downstream of the shock we expect equipartition between the particles and magnetic field to be reached, so that $B^2/4\pi = P$, where B is the mean magnetic field in the nebula. We then estimate a value of $B \gtrsim 100 d_{2.7}^{-1} \mu\text{G}$. The corresponding synchrotron lifetime of particles emitting at an energy ϵ_{keV} (in units of keV) is very small, at $t_{\text{synch}} \lesssim 40 d_{2.7}^{3/2} \epsilon_{\text{keV}}^{-1/2}$ yr. The velocity that is needed for these particles to reach the edge of the nebula within their synchrotron lifetimes is $v \gtrsim 2,600 d_{2.7}^{-1/2} \epsilon_{\text{keV}}^{1/2} \text{ km s}^{-1} \gtrsim 0.01 d_{2.7}^{-1/2} \epsilon_{\text{keV}}^{1/2} \text{ c}$.

One problem with the above interpretation is that we expect the emission downstream of the shock to be symmetric about the pulsar. A possible explanation for the lack of emission to the NW involves Doppler boosting of the approaching (in this case SE) component. The observed flux ratios on either side of the pulsar require an intrinsic expansion velocity of $v \sin \theta \gtrsim 0.22c$, where θ is the inclination of the nebula to the line of sight. Simi-

lar velocities are found in the structures of other PWNe, such as the Crab (Hester et al. 2002). An intrinsically asymmetric pulsar wind could also be responsible for the observed characteristics.

The emission in the body of the nebula could also represent a collimated outflow, or jet, along the pulsar spin axis, as observed in other systems such as the Crab and Vela (Weisskopf et al. 2000; Helfand et al. 2001). In this case, we can estimate the minimum magnetic field and energy needed to support the jet against the surrounding pressure using equipartition arguments (e.g., Pacholczyk 1970; Seward et al. 1984). We assume the jet to be a cylinder with length $l_j = 6.5'' = 0.085 d_{2.7}$ pc and radius $r_j = 1.5'' = 0.020 d_{2.7}$ pc, resulting in an emitting volume of $V \sim 3 \times 10^{51} d_{2.7}^3 \text{ cm}^3$. From the results shown in Tables 1 and 2, we infer an unabsorbed jet luminosity in the 0.5–10.0 keV range of $L_j > 2 \times 10^{31} \text{ ergs s}^{-1}$ (1σ limit). Equipartition arguments ($B \propto L^{2/7} V^{-2/7}$, $E \propto B^2 V$) then imply a magnetic field in the jet of $B_j > 42 (1+\mu)^{2/7} \phi^{-2/7} \mu\text{G}$ and an energy of $E_j > 4.4 \times 10^{41} (1+\mu)^{4/7} \phi^{3/7}$ ergs. Here, μ is the ratio of ion to electron energy and ϕ is the filling factor in the jet. We note that these represent very conservative lower limits on B_j and E_j , as the total emission from the jet can have a significant contribution at lower energies. Using the above limit on B_j , the corresponding synchrotron lifetime for particles emitting at 2 keV is $t_j < 100 (1+\mu)^{-3/7} \phi^{3/7}$ yr and implies a velocity in the jet of $v_j > 1,000 (1+\mu)^{3/7} \phi^{-3/7} \text{ km s}^{-1}$.

For the Crab and Vela, the nebular magnetic field has been estimated to be ~ 100 's μG (e.g., Aharonian et al. 2004; Pavlov et al. 2001a). Similar fields have also been found for the large-scale jet in Vela (Pavlov et al. 2003). These are consistent with our derived fields above, suggesting the presence of similar confining pressures. The size and energetics of the nebula surrounding PSR B1046–58 are similar to that of Vela, as expected if these properties are also related to the pulsar's spin-down energy \dot{E} . In contrast, the nebula surrounding PSR B1509–58 (Gaensler et al. 2002) shows much smaller equipartition fields ($\sim 8 \mu\text{G}$) and larger size, pointing to a smaller confining pressure.

An alternate argument for an asymmetric nebula involves the confinement of the pulsar wind due to the ram pressure of a fast-moving pulsar (e.g., Gaensler et al. 2004). In this case, the body of the nebula would represent the expected X-ray tail aligned with the bow shock axis in the direction opposite to the pulsar proper motion. The implied position angle in the plane of the sky of the proper motion would be $\sim 310^\circ$ (measured east of north). Recent *Chandra* observations of the Geminga pulsar revealed a somewhat similar morphology for its PWN (Pavlov et al. 2005; de Luca et al. 2006) which is likely to arise due to the high space velocity of the pulsar.

In the case of a high space velocity, the confining pressure for the nebula is given by $P = \rho V^2$, where ρ is the ambient density and V is the pulsar's speed. For cosmic abundances and a number density n_0 in the ambient medium we get $\rho = 1.37 n_0 m_H = 2.3 \times 10^{-24} n_0 \text{ g cm}^{-3}$, where n_0 is in units of 1 cm^{-3} . Our above estimate for P results in a velocity of $V \gtrsim 190 n_0^{-1/2} \text{ km s}^{-1}$. Such a velocity is consistent with estimates for other bow-shock nebulae (e.g., Chatterjee & Cordes 2002) and the

⁹ Gotthelf (2004) has later suggested that this relationship only holds for pulsars with $\dot{E} > 4 \times 10^{36} \text{ ergs s}^{-1}$ and without a bow-shock morphology.

expected distribution of pulsar velocities at birth (Arzoumanian et al. 1994; Faucher-Giguere & Kaspi 2005). The proper motion for the pulsar in this case would be $\gtrsim 0''.015 d_{2.7}^{-1} \text{ yr}^{-1}$ and could be detected by radio interferometry. We note that a bow-shock interpretation for the X-ray morphology would differ from the static PWN interpretation favoured to explain the non-detection of an extended radio nebula (Stappers et al. 1999). A consistent bow-shock interpretation in both radio and X-rays is possible if the undetected radio nebula is unresolved with $r_{s,radio} \lesssim 10''$ and has a low efficiency of $\eta_R \sim 10^{-6}$, which results in estimates from the radio observations of $V \sim 250 \text{ km s}^{-1}$ and $n_0 \sim 0.1 \text{ cm}^{-3}$ (Stappers et al. 1999).

As suggested above, the structures observed in the body of the nebula can represent emission due to particles left behind after the passage of the pulsar for a large enough velocity. For $V > 190 \text{ km s}^{-1}$, the time taken by the pulsar to travel the observed distance is $< 540 d_{2.7}^2 \text{ yr}$. Synchrotron lifetimes matching this limit require magnetic fields of $B \gtrsim 20 \mu\text{G}$ at 1 keV. This is consistent with the above equipartition field expected to hold in the vicinity of the pulsar given the uncertainties in our estimates above. The emission from the body and the north clump could also contain contributions from high velocity outflows. The north clump at a radius $\sim 3''$ from the pulsar “ahead” of the bow is not expected to arise due to shocked ambient medium. For example, at a velocity $V = 190 d_{2.7}^{-1} \text{ km s}^{-1}$ and density $n_0 = 1 \text{ cm}^{-3}$, the medium is expected to have a temperature $kT \sim 0.07 n_0^{-1} \text{ keV}$. The luminosity is expected to be $L_X \sim \Lambda n_0^2 V' \text{ ergs s}^{-1} \sim 10^{28} n_0^2 d_{2.7}^3 \text{ ergs s}^{-1}$, where $\Lambda \sim 1.3 \times 10^{-24} n_0^{-1/2} \text{ ergs cm}^3 \text{ s}^{-1}$ is the cooling function at $kT \sim 0.07 n_0^{-1} \text{ keV}$ and $V' \sim 7 \times 10^{51} d_{2.7}^3 \text{ cm}^3$ is the volume of the shocked gas within $3''$ of the pulsar (see, e.g., Rybicki & Lightman 1979; Gaensler et al. 2004). The implied absorbed flux at Earth is then much smaller than the measured values. Additional observations can be used to confirm the presence of the north clump and its association to the system.

6.3. PSR B1046–58 and 2EG J1049–5827

Although not confirmed, an association between PSR B1046–58 and 2EG J1049–5827 has been proposed in light of, among other things, their positional coincidence, possible γ -ray pulsations, and spectral and energetic properties of the γ -ray pulsar (Fierro 1995; Pivovaroff et al. 2000a; Kaspi et al. 2000). 2EG J1049–5827 was found to have a pulsed γ -ray flux above 400 MeV of $(2.5 \pm 0.6) \times 10^{-10} \text{ ergs cm}^{-2} \text{ s}^{-1}$, implying a γ -ray efficiency of $(9 \pm 2) \times 10^{-3}$ (for 1 sr beaming and a distance of 2.7 kpc, Kaspi et al. 2000). Unresolved, unpulsed γ -ray emission at the pulsar position was also found.

An extrapolation of the observed X-ray spectrum for PSR B1046–58 and its PWN (see Table 2) to energies $> 400 \text{ MeV}$ predicts a flux of $0.7 \times 10^{-13} \text{ ergs cm}^{-2} \text{ s}^{-1}$, three orders of magnitude lower than that derived for the EGRET source. This is true for other well-established γ -ray pulsars (e.g., Thompson et al. 1999). Observations at higher X-ray energies (e.g., deep exposures using *RXTE*, *Suzaku*) can help determine whether PSR B1046–58 is indeed a γ -ray pulsar by detecting possible high X-ray energy pulsations and spectral characteristics consistent

with those of 2EG J1049–5827.

We note the presence of a particularly hard X-ray source visible in the *Chandra* data, $\sim 3/3$ from the pulsar position at coordinates $\alpha_{2000} = 10^h 48^m 05^s 74 (\pm 0.15)$ and $\delta_{2000} = -58^\circ 28' 46'' (\pm 2.4)$. The source is coincident with “Src 4” in Pivovaroff et al. (2000a); see also Figure 3. A total of 164 ± 15 counts were detected from this source and its spectrum is well described by a non-thermal power-law model with $N_H = (0.7^{+0.4}_{-0.2}) \times 10^{22} \text{ cm}^{-2}$, $\Gamma = 1.1^{+0.3}_{-0.2}$ and unabsorbed flux in the 0.5 – 10.0 keV of $(1.2^{+0.5}_{-0.4}) \times 10^{-13} \text{ ergs s}^{-1} \text{ cm}^{-2}$ ($\chi^2 = 0.45$ for 5 d.o.f., 1σ errors). No counterpart for this source was found at other wavelengths and it lies within the 99% confidence error of 2EG J1049–5827. This suggests that the observed γ -ray emission could have contributions from more than one source. Higher spatial resolution γ -ray observations with future missions may help to address this possibility.

We also find that the emission from the nebula dominates at high X-ray energies (see Table 1) over that of the pulsar. This argues for the unpulsed γ -ray emission associated with 2EG J1049–5827 to also arise, at least in part, from the nebula, as proposed for the Vela and Crab pulsars (Nolan et al. 1993; Kanbach et al. 1994; Fierro et al. 1998).

6.4. Non-detection of a Supernova Remnant

As we do not detect emission from a supernova remnant (SNR) in the field containing PSR B1046–58, following Gaensler et al. (2003) we can estimate the flux from a possible unseen remnant by scaling the emission observed from the Vela SNR. The emission from this remnant can be described by a two-component Raymond-Smith plasma with temperatures $kT_1 \sim 0.15 \text{ keV}$ and $kT_2 \sim 1 \text{ keV}$ (Lu & Aschenbach 2000). The total unabsorbed luminosity in the 0.1 – 2.4 keV range is $2.2 \times 10^{35} \text{ ergs s}^{-1}$ and the cooler component has a volume-integrated emission measure ~ 10 times higher than the hot component. Scaling to a distance of 2.7 kpc, the unabsorbed flux densities for each component would be $f_1 = 2.3 \times 10^{-10} \text{ ergs s}^{-1} \text{ cm}^{-2}$ and $f_2 = 2.2 \times 10^{-11} \text{ ergs s}^{-1} \text{ cm}^{-2}$, respectively.

The expected ACIS-S¹⁰ count rate predicted by the WebPIMMS tool¹¹ is $< 2.6 \text{ counts s}^{-1}$ (on-axis) for absorbing columns $> 5 \times 10^{21} \text{ cm}^{-2}$. Scaling the size of the Vela SNR ($\sim 8^\circ$ at 300 pc, Lu & Aschenbach 2000), we would expect a shell with a radius of $\sim 26'$ at 2.7 kpc. This size is larger than the ACIS-S (and EPIC-MOS) field of view. However, parts of the remnant might be visible in the present data given the uncertainties in the spatial distribution of the remnant and direction of motion of the pulsar. Assuming emission areas for the remnant proportional to having a shell thickness $> 20\%$ of its radius, the expected surface brightness density is $\lesssim 0.8 \times 10^{-6} \text{ counts s}^{-1} \text{ arcsec}^{-2}$. This is lower than the ACIS-S background level during the observation, estimated to be ~ 2 – $6 \times 10^{-6} \text{ counts s}^{-1} \text{ arcsec}^{-2}$ (accounting for vignetting at large off-axis angles).

¹⁰ The EPIC-MOS data provide less constraining limits for this emission due to their lower sensitivity and higher background levels. The EPIC-PN data had a much smaller exposure time and limited field of view.

¹¹ <http://heasarc.gsfc.nasa.gov/Tools/w3pimms.html>

It is then possible that a remnant with similar properties to that of the Vela remnant might be present and it is undetected by these observations. The lack of radio or X-ray emission from the SNR has also been attributed to an initial fast expansion into a low-density cavity (e.g., Braun et al. 1989). This expansion is followed by a collision with a dense surrounding shell of stellar wind material from the progenitor where the emission fades rapidly and energy is dissipated through radiative shocks.

7. CONCLUSIONS

We have detected an asymmetric, arc-second scale PWN surrounding the young, energetic PSR B1046–58. The overall emission from the pulsar and PWN is best described by a non-thermal power-law model with $\Gamma=1.7^{+0.4}_{-0.2}$ and a low X-ray luminosity of $\sim 10^{32}$ ergs s $^{-1}$ in the 0.5–10.0 keV range. The brightest emission region in the PWN is coincident with the radio coordinates of the pulsar. It is resolved as an extended structure with *Chandra* and we suggest that it can represent an upper limit to the location of the wind termination shock. The additional, asymmetric structures can represent nebular emission downstream of the shock or collimated outflow from the pulsar. The implied equipartition magnetic fields are $\gtrsim 40$ –100 μ G. The overall size and energetics of the system in this case are very similar to those of the Vela pulsar. Instead, if the observed asymmetry in the nebula were to arise due to a large space velocity for the pulsar we estimate a value of $\gtrsim 190 n_0^{-1/2}$ km s $^{-1}$. In this case, we would favor the presence of arcsecond-scale nebulae with low efficiencies in both X-ray and radio.

Our spatially resolved analysis also hints at the presence of softer emission from the pulsar than from the rest of the nebula. In the case that thermal emission from the whole surface of the star is present, we derive an upper limit for the temperature of $<1.4 \times 10^6$ K, which is not constraining on cooling models of neutron stars. In the case of a small hot spot on the surface, the implied temperature is $>2.5 \times 10^6$ K and would be consistent with those seen for other pulsars.

The results shown here demonstrate the need for high-resolution, high-sensitivity observations in order to study the wide range of structures associated with rotation-powered pulsars. While the origin of these structures cannot be unambiguously determined in the case of PSR B1046–58, they can be broadly understood using current theories for the production PWNe. Additional data and theoretical work are needed to reach a consistent picture of this interesting phenomenon in neutron star physics.

This work was supported in part by an NSERC Discovery Grant and Steacie Supplement, FQRNT, NSERC Graduate Scholarship and a Canadian Institute for Advanced Research Fellowship, the Canada Research Chair Program, SAO grant GO3-4068X awarded by the CXC and by NASA grant NAG5-11376 awarded by NASA's XMM Guest Observatory Facility. B.M.G. acknowledges the support of NASA through LTSA grant NAG5-13032, and of an Alfred P. Sloan Research Fellowship. We thank R. N. Manchester for kindly providing the Parkes radio ephemeris for PSR B1046–58.

REFERENCES

Aharonian, F., et al. 2004, ApJ, 614, 897

Arzoumanian, Z., Nice, D. J., Taylor, J. H., & Thorsett, S. E. 1994, ApJ, 422, 671

Braun, R., Goss, W. M., & Lyne, A. G. 1989, ApJ, 340, 355

Buccieri, R., et al. 1983, A&A, 128, 245

Camilo, F., et al. 2004, ApJ, 616, 1118

Chatterjee, S., & Cordes, M., J. 2002, ApJ, 575, 407

Cordes, J. M., & Lazio, T. J. W. 2002, ApJ, submitted, (astro-ph/0007310)

Cutri, R. M., et al. 2003, VizieR Online Data Catalog II/246

de Luca, A., et al. 2006, A&A, 445, L9

Faucher-Giguere, C. .., & Kaspi, V. M. 2005, ApJ, submitted, (astro-ph/0512585)

Fierro, J. M. 1995, Ph.D. thesis, Stanford University

Fierro, J. M., Michelson, P. F., Nolan, P. L., & Thompson, D. J. 1998, ApJ, 494, 734

Frail, D. A., & Scharringhausen, B. R. 1997, ApJ, 480, 364

Gaensler, B. M., et al. 2002, ApJ, 569, 878

Gaensler, B. M., et al. 2003, ApJ, 588, 441

Gaensler, B. M., & Slane, P. O. 2006, ARAA, 44, 17

Gaensler, B. M., et al. 2000, MNRAS, 318, 58

Gaensler, B. M., et al. 2004, ApJ, 616, 383

Garmire, G. P., et al. 2003, Proc. SPIE, 4851, 28

Gotthelf, E. V. 2003, ApJ, 591, 361

Gotthelf, E. V. 2004, in IAU Symposium, ed. F. Camilo & B. M. Gaensler, 225

Helfand, D. J., Gotthelf, E. V., & Halpern, J. P. 2001, ApJ, 556, 380

Hester, J. J., et al. 2002, ApJ, 577, L49

Johnston, S., et al. 1992, MNRAS, 255, 401

Kanbach, G., et al. 1994, A&A, 289, 855

Kaspi, V. M., et al. 2000, ApJ, 528, 445

Kaspi, V. M., Roberts, M. S. E., & Harding, A. K. 2004, in Compact Stellar X-ray Sources, ed. W. H. G. Lewin & M. van der Klis (UK: Cambridge University Press), in press (astro-ph/0402136)

Lu, F. J., & Aschenbach, B. 2000, A&A, 362, 1083

Monet, D. G., et al. 2002, VizieR Online Data Catalog

Nolan, P. L., et al. 1993, ApJ, 409, 697

Pacholczyk, A. G. 1970, Radio Astrophysics (San Francisco: Freeman)

Page, D., Geppert, U., & Weber, F. 2005, to be published in Nucl. Phys. A (astro-ph/0508056)

Pavlov, G. G., Kargaltsev, O. Y., Sanwal, D., & Garmire, G. P. 2001a, ApJ, 554, L189

Pavlov, G. G., Sanwal, D., & Zavlin, V. E. 2005, ApJ, submitted, astro-ph/0511364

Pavlov, G. G., Teter, M. A., Kargaltsev, O., & Sanwal, D. 2003, ApJ, 591, 1157

Pavlov, G. G., Zavlin, V. E., & Sanwal, D. 2002, in Proc. 270th WE-Heraeus Seminar on Neutron Stars, Pulsars, and Supernova Remnants, ed. W. Becker, H. Lesch, & J. Trümper (MPE Rep. 278; Garching: MPE), 273 (astro-ph/0206024)

Pavlov, G. G., et al. 2001b, ApJ, 552, L129

Pivovaroff, M., Kaspi, V. M., & Camilo, F. 2000b, ApJ, 535, 379

Pivovaroff, M., Kaspi, V. M., & Gotthelf, E. V. 2000a, ApJ, 528, 436

Ransom, S. M., Gaensler, B. M., & Slane, P. O. 2002, ApJ, 570, L75

Raymond, J. C., & Smith, B. W. 1977, ApJS, 35, 419

Rybicki, G. B., & Lightman, A. P. 1979, Radiative Processes in Astrophysics (New York: Wiley)

Seward, F. D., Harnden Jr., F. R., Szymkowiak, A., & Swank, J. 1984, ApJ, 281, 650

Stappers, B. W., Gaensler, B. M., & Johnston, S. 1999, MNRAS, 308, 609

Strüder, L., et al. 2001, A&A, 365, L18

Thompson, D. J., et al. 1999, ApJ, 516, 297

Turner, M. J. L., et al. 2001, A&A, 365, L27

Vaughan, B. A., et al. 1994, ApJ, 435, 362

Voges, W., et al. 2000, VizieR Online Data Catalog IX/29

Weisskopf, M. C., et al. 2000, ApJ, 536, L81

Woods, P. M., et al. 2004, ApJ, 605, 378

TABLE 1
SPATIAL ANALYSIS OF PSR B1046–58 AND ITS PWN WITH *Chandra*

Region	0.5–2.0 keV counts (S)	2.0–10.0 keV counts (H)	HR = (S–H)/(S+H)	S/N (0.5–10.0 keV)
Pulsar (1" radius ^a)	43 ± 8	24 ± 6	0.27 ± 0.10	8.5 σ
PWN, all (- Pulsar)	46 ± 9	70 ± 11	−0.21 ± 0.06	9.1 σ
PWN, “head” (- Pulsar)	12 ± 5	31 ± 7	−0.44 ± 0.21	6.1 σ
PWN, “body”	22 ± 6	34 ± 7	−0.22 ± 0.10	9.1 σ
“North clump”	5 ± 2	5 ± 2	0.00 ± 0.02	2.9 σ
Pulsar + PWN	89 ± 11	95 ± 12	−0.03 ± 0.01	12.1 σ

^aSee §3 for detailed discussion.

TABLE 2
POWER-LAW FIT TO COMBINED EMISSION
FROM PSR B1046–58 AND ITS PWN^a

Parameter	Value ($\pm 1\sigma$)
N_H (10 ²² cm ^{−2})	0.9 ^{+0.4} _{−0.2}
Γ	1.7 ^{+0.4} _{−0.2}
χ^2 (dof)	79(68)
f_{abs} ^b (ergs s ^{−1} cm ^{−2})	0.7 ^{+0.6} _{−0.1} × 10 ^{−13}
f_{unabs} ^b (ergs s ^{−1} cm ^{−2})	1.0 ^{+0.7} _{−0.2} × 10 ^{−13}
L_X ^c (ergs s ^{−1})	0.9 ^{+0.6} _{−0.2} × 10 ³²

^aSimultaneous fit to both *Chandra* and *XMM-Newton* spectra.

^bAbsorbed and unabsorbed X-ray fluxes, f_{abs} and f_{unabs} , in the 0.5–10.0 keV range.

^cUnabsorbed X-ray luminosity in the 0.5–10.0 keV range for a distance of 2.7 kpc.